Meteorol. Z. (Contrib. Atm. Sci.), Vol. 33 (2024), 475–488
Published online January 29, 2025

Open Access
Boundary Layer Meteorology

Mesoscale simulations of coastal boundary-layer transitions. Part 2: offshore wind speed development

Mares Barekzai[1,*], Beatriz Cañadillas[2], Stefan Emeis[1], Martin Dörenkämper[3], Astrid Lampert[2]

[1] Institute of Meteorology and Climate Research – Atmospheric Environmental Research (IMK-IFU), Karlsruhe Institute of Technology (KIT), Garmisch-Partenkirchen, Germany
[2] Institute of Flight Guidance, TU Braunschweig, Braunschweig, Germany
[3] Fraunhofer Institute for Wind Energy Systems, Oldenburg, Germany
* Corresponding author: mares.barekzai@posteo.de

With 7 figures and 3 tables

Abstract: The share of wind energy in the global electricity supply continues to grow, with offshore wind farms near coastlines forming a major part of this growth. High quality wind forecasts are needed for coastal areas, where wind directions from land towards the sea are associated with high variability. This raises two questions: How far offshore does the impact of the coastal transition reach, and how large is the impact on the wind resource? To address these questions, this article analyzes a 12-year data set (between 2010 and 2021) of mesoscale simulations performed with the Weather Research and Forecast Model (WRF) over the German Bight. The simulation results are evaluated using a comprehensive statistical approach for all wind directions and, additionally, only for wind directions from land to sea (offshore wind directions, defined here as wind directions from the South, Southeast, and East). The interannual variability of wind speed averaged over each of the 12 years is in the order of 1 m s^{-1} for all wind directions and up to 1.5 m s^{-1} for only offshore wind directions.

On average, the coastal impact decreases with height and with increasing absolute wind speed. For all wind directions, the wind speed gradients are most pronounced close to the coastline, and decrease with distance from the coast until reaching a new equilibrium wind speed. For the selected offshore wind directions, which occur approximately 30% of the time for the 12-year data set, a consistent linear increase in wind speed with distance was observed above sea. For all wind directions, 95% of the reference wind speed at 200 km distance from the coast was reached after 60 km (40 km, 30 km) for a height of 10 m (100 m, 200 m). For only offshore wind directions, 95% of the wind speed at 200 km distance from the coast was reached after 100 km (120 km, 130 km) for a height of 10 m (100 m, 200 m).

The results of the spring, summer, and daytime simulations are similar in terms of the horizontal extent of the coastal effect and the increase of wind speed. The horizontal extent increases with height and reaches a distance of 180 km at a height of 200 m. Winter, autumn, and nighttime simulations are similar in that the horizontal extent of wind speed increase is limited to a distance of approximately 50 km up to a height of 200 m. The impact of the coastal effect on wind speed decreases with height. For wind directions from Southeast, the linear increase in wind speed does not level off even at a distance of 200 km.

The wind speed development for wind directions from the Southeast shows the most symmetric behavior for the coastal effect, with wind speed increasing gradually from the southern and eastern coastlines to the open sea. The wind speed development for wind directions from the East and South shows geolocation-specific features. The wind from the East shows a tunnel effect induced by the geometry of the Danish landmass, while the wind speed for wind directions from the South increases more quickly towards the West along the Dutch coast.

Keywords: WRF; offshore; German Bight; coastal effect; wind energy; internal boundary layer; SDG7

1 Introduction

The transformation of the energy sector towards regenerative sources strongly relies on wind energy (International Energy Agency 2022). In particular offshore wind energy experiences a large expansion of wind farm areas and installed capacity: For example in Germany, according to the recent governmental decisions in 2022, it is planned to install a capacity of 30 GW in the Exclusive Economic Zone of North Sea and Baltic Sea until 2030, and even 70 GW until 2045

DOI: 10.1127/metz/2024/1196
Gebrüder Borntraeger Science Publishers, Stuttgart, www.borntraeger-cramer.com

(International Energy Agency 2022). For the efficient usage of offshore wind farm areas and reliable feed-in planning, it is essential to have precise knowledge of the available wind resource at the planned site, and to have reliable forecasts of the wind speed on the scale of hours and days. Operational weather forecast is used for hourly and day-ahead planning of the expected energy output. As the desired accuracy of wind speed is around 3% (European Wind Energy Association 2013), knowledge about the wind speed gradient from the coast to the open sea for offshore wind directions is important to improve the forecast. Despite the expected drastic decline in wind energy cost (Wiser et al. 2021), all phenomena significantly reducing or enhancing the energy yield have to be considered carefully for the operation of current and the planning of future wind parks (Akhtar et al. 2021), and included in economic efficiency calculations (Lundquist et al. 2019).

Due to spatial limitations and for sharing expensive infrastructure, offshore wind turbines are mostly arranged as wind farms containing up to 100 individual turbines, and as large clusters of the dimensions of several 10 km to 100 km combining different wind farms (Schulz-Stellenfleth et al. 2022a). Ideas for using floating platforms or different foundation mechanisms at larger water depth are currently investigated (e.g., Manzano-Agugliaro et al. 2020). For economic and logistical reasons, like shallower water depth and less cost for cable installations, most wind farm areas are typically located within distances of several tens of kilometers off the coast. Depending on wind direction, they are therefore frequently influenced by coastal effects (Schulz-Stellenfleth et al. 2022b; Djath et al. 2022).

Currently, there are different challenges related to the assessment of the wind resource for offshore locations: The coastal effect, which is the modification of the wind field for air masses passing the transition from land to sea, is a complex phenomenon, depending on the distribution of high and low pressure systems, wind direction, the different surface roughness between land and sea, temperature differences between surface and air masses, and in particular atmospheric stability. There are more specific phenomena developing at the coast: The sea breeze is an additional circulation pattern induced by thermal contrasts above land and open water (see, e.g., Chapter 5 in Atkinson 1981). Sea breeze effects vary strongly with location at the North Sea coasts, and different subtypes are associated with different wind speed increase (Steele et al. 2015). Depending on the site and prevailing wind mechanisms, sea breeze events can significantly influence wind energy production, e.g. in India with generally low wind speed during monsoon season (Kumar et al. 2021). Low-level jets, consisting of an increase of wind speed with height and subsequent decrease, develop during the formation of stable conditions, e.g., when warm air is advected over the colder sea surface (Smedman et al. 1993, 1997).

All these effects strongly depend on atmospheric stability, which is determined by the vertical distribution of temperature and humidity. Vertical profile information of these parameters is highly important, but only sparsely available at a few measurement masts in the German Bight of the North Sea, at the research platforms FINO1 (Muñoz-Esparza et al. 2012a; Cheynet et al. 2022) and FINO3 (Gualtieri 2021; Gottschall & Dörenkämper 2021), during radiosonde ascents (Rausch et al. 2022), or by dedicated measurements, like airborne investigations (Lampert et al. 2020, 2024). To complement measurements, high resolution numerical simulations play an important role in studying the wind resource.

Orographic effects, like the coastal effect (van der Laan et al. 2017) with different fetch length, defined as the distance to the coast along the wind direction, result in strong horizontal gradients of wind speed, and introduce uncertainty in simulations (Lee & Lundquist 2017; Siedersleben et al. 2018). The development of atmospheric stratification from land to the sea cannot be captured correctly in numerical simulations (Sandu et al. 2013), producing large uncertainties in the representation of wind park effects (Siedersleben et al. 2018).

This study addresses the following questions of relevance for wind energy and for understanding flow conditions in coastal areas based on a high resolution data set:

- What is the horizontal extent of the influence of the coastal transition on the wind field?
- How significant is the impact of the coastal transition on the wind field at different altitudes?
- How is the impact of the coastal transition related to time of day and season?

This article is the second of two partner papers, with the general scope to analyze the changes in the wind field for flow from land to the open ocean for offshore wind directions in the German Bight. From a whole 12-year data set, it extracts the wind directions influenced by the coastal effect, which are wind from south (S), southeast (SE) and east (E), and compares statistics of wind speed development to the entire data set. The partner paper (Barekzai et al. 2024) has a specific focus on the spatial distribution of low-level jet occurrence. In contrast, this article investigates the coastal transition of the offshore wind speed development based on numerical simulations with the Weather Research and Forecast model (WRF) version 4.2.1. In particular, it analyses the influence of wind direction on the increase in wind speed with fetch length, and distinguishes different seasons and times of day as an indicator for atmospheric stability. The study focuses on quantifying the wind speed gradient from the coast to the open sea for different altitudes and wind directions. A better understanding of the spatial and temporal variability of the coastal effect is important for improving the accuracy of wind energy forecasts, which should be better than about 3%. The findings from this study could contribute to achieving this goal by providing information that can

be used to enhance forecasting models. The high resolution of the simulations is crucial for achieving realistic results in transition areas. While the accuracy of wind speed forecasts is relevant, it is not the primary focus of the study.

The manuscript is structured as follows: Sect. 2 provides an overview of the model setup, of the distribution of the model data into sectors of wind direction, and of the methods used for data processing. Sect. 3 provides the key results of the wind field analyses, which are discussed in Sect. 4. A conclusion is drawn in Sect. 5.

2 Methods

2.1 WRF setup

The WRF model version 4.2.1 (Skamarock et al. 2019) was used for mesoscale simulations to predict various atmospheric variables in the German Bight area, including, e.g., horizontal wind components, potential temperature, geopotential, surface pressure of dry air, water vapor, and cloud water. The WRF model is widely used in the wind energy community (Hasager et al. 2020; Li et al. 2021; Larsén et al. 2024) and for wind farm wake analyses (Larsén & Fischereit 2021; Platis et al. 2021). A nested domain approach was used, with resolutions of 18 km, 6 km, and 2 km, to reduce computational cost. The boundary conditions for atmospheric and sea surface variables were prescribed using the ERA5 and OSTIA datasets, respectively. The vertical resolution is 25 m up to the altitude of 200 m, and 50 m up to the altitude of 400 m, plus the altitude of 500 m and 1000 m. The temporal resolution is 15 min. The setup was optimized within several research projects for wind energy applications, especially with a focus on offshore conditions (Dörenkämper et al. 2020; Gottschall & Dörenkämper 2021).

High resolution simulations, obtained without the use of wind farm parameterization or data assimilation, were conducted over the southern North Sea for a 12-year period from 2010 to 2021, as this time period is of high interest for the wind energy industry, with a growing number of wind parks in operation in the exclusive economic zone of Germany in the North Sea. The high spatial resolution is crucial for realistically representing the complex flow conditions in coastal areas, which are the focus of this study. The transition from land to sea leads to strong horizontal gradients in wind speed and the development of a stably stratified internal boundary layer, which cannot be adequately captured by models with low resolution. This leads to significant uncertainties in simulating wind effects, which are critical for wind energy production. More details about the model configuration decisions can be found in Table 1. Interested readers are referred to the partner paper for more information (Barekzai et al. 2024).

Cañadillas et al. (2023) compared these model results at two locations, on the German coast (53 ° 42.75′N, 7 ° 9.13′E) and at the FINO1 mast (54 ° 0.864′N, 7 ° 35.262′E), with wind lidar measurements to assess the performance of the model in capturing the wind speed distribution. The comparison showed that the model performs reasonably well and captures the general trend of wind speed and its gradients in coastal areas despite some inherent differences due to factors such as spatial resolution, atmospheric conditions, and model assumptions.

Table 1. Relevant parameters of the mesoscale model set-up. The references for the different schemes and models are summarized in (WRF Users Page, 2020).

Parameter	Setting
WRF model version	4.2.1
Planetary Boundary Layer (BLH) scheme	MYNN level 2.5
Land use data	MODIS
Surface layer scheme	MYNN
Microphysics scheme	WRF Single-Moment 5-class
Shortwave and long-wave radiation	RRTMG
Atmospheric boundary conditions	ERA5
Sea surface conditions	OSTIA
Horizontal resolution	18 km, 6 km, 2 km
Vertical resolution	60 eta-level
Nudging	grid nudging above BLH
Model output interval	10 min
Nesting	one-way
Land surface model	Unified Noah Land Surface Model
Simulation duration	240 (+24 spin-up) hours

2.2 Transect analysis

The wind speed datasets were divided into 45-degree wind direction sectors. For the entire dataset and a subset containing only three wind directions blowing from land over the North Sea (S, SE, and E, collectively referred to as “offshore” wind directions), several parallel transects of 50 km width were defined along each direction and labeled as S1–3, SE1–4, and E1–5 (Fig. 1).

To analyze the grid cells within the transects, the atmospheric variables were averaged perpendicular to the alignment of each transect. These averages were then combined by taking the mean along the transects, and the standard deviation over the transects was determined. This approach enables the investigation of the horizontal development of the atmospheric boundary layer, specifically the wind profile with fetch length, based on statistically representative datasets. The transects were aligned based on the average position of the coastal transition of the respective transect. To carry

out the analysis, the dataset was divided by principal wind direction (S, SE, E), height (10 m, 100 m, 200 m), individual years between 2010 and 2021, day and nighttime, and season. The seasons were divided into spring (March, April, May), summer (June, July, August), autumn (September, October, November) and winter (December, January, February). The analyses distinguish between day and night time based on the true sunrise and sunset at the center coordinate of the investigation area for each individual day.

It should be noted that the standard deviation of the wind speed is lower when the entire data set is considered than when only specific wind directions are taken into account.

3 Results

The following results are averaged over the southern North Sea for a period of 12 years. The offshore wind directions for the German Bight, with air mass flow from land over the sea, are South (S), East (E), and Southeast (SE), which together occur in approximately 30% of the time over the study period. More details on the distribution of wind directions can be found in Part 1 of the manuscript (Barekzai et al. 2024).

The following analyses of the wind field identify how far the coastal transition extends until a new equilibrium wind speed is reached above the open water, and how strong the wind speed increase is in relation to the fetch length.

3.1 Spatial distribution of coastal wind speed

Fig. 1a shows the averaged 2D wind field for all wind directions evaluated at an altitude of 100 m. The panels b, c and d of Fig. 1 show the same as 1a but for easterly, southerly and south-easterly wind directions, respectively. Furthermore, the panels b, c and d show the transect areas labelled with S1–3, SE1–4 and E1–5, which are the base for the subsequent analyses.

As expected, the wind speed is generally lower above the coast than above the open ocean. For all wind directions (Fig. 1a), the gradient in wind speed follows the shape of the coastline, but is more pronounced at the southerly coast in the direction of the prevailing wind, as indicated by the arrows. For easterly wind directions (Fig. 1b), the wind field shows a faster increase of the wind speed with higher values of 10 m s^{-1} at a latitude of 54 °N, where the landmass to the east is the thinnest. Here, higher wind speed is found close to the shore.

For southerly wind directions (Fig. 1c), the wind gradient extends farther off the coast in the east than in the west, reflecting the east-west gradient of wind speed above land, and possibly influenced by longer overland travel times and higher topography in the east. For south-easterly wind directions (Fig. 1d), the lines of constant wind speed closely map the shape of the coastline, and the impact of the coastal transition on the wind field can be estimated to reach 200 km offshore. The results for wind directions from E and S show very geolocation specific features, while the results for wind from SE show a continuous increase in wind speed along both coastlines.

3.2 Coastal wind speed development with fetch

Fig. 2 illustrates the development of wind speed with distance from the coast for the different altitudes (10 m, 100 m, and 200 m), averaged over the transects marked in Fig. 1b, c and d. Fig. 2a is averaged over all wind directions, while Fig. 2b is averaged over the selected wind directions (E, SE, S). Both panels show that the average wind speed increases with height up to an altitude of 200 m, but the influence of the surface and, consequently, the coastal gradient decreases with height. The coastal gradient is strongest at 10 m with a wind speed increase of about 4 m s^{-1} after 200 km offshore.

For all wind directions (Fig. 2a), the maximum wind speed gradient is closer to the coastline and flattens after 50 km. In contrast, the gradient for offshore wind directions (Fig. 2b) does not flatten, but continues to increase linearly farther offshore. A similar development of wind speed from the coast to the sea, depending on the wind direction, was found by Cañadillas et al. (2023), where only southerly wind directions were analyzed in the same study area using ERA5 model data.

In summary, the main difference between all wind directions and only offshore wind directions is the distance that the offshore coastal effect reaches: For all wind directions, the wind speed reaches 95% of the wind speed at the reference distance of 200 km after 60 km (35 km, 20 km) for the altitude of 10 m (100 m, 200 m), see summary in Table 2. In contrast, for offshore wind directions, the wind speed reaches 95% of the wind speed at a distance of 200 km after a distance of 100 km (110 km, 115 km), see Table 3.

3.3 Coastal wind speed gradient for offshore wind directions

Fig. 3 shows the wind speed development at a height of 100 m, averaged separately over the transects S, SE and E, which are highlighted in Fig. 1. For all wind directions (Fig. 3a), the coastal gradients for all transect directions level off after 100 km distance from the coast. For offshore wind directions (Fig. 3b), the wind development is evaluated for the same wind directions as the transect orientations E, SE, and S. For wind directions from SE, the wind speed increases strongly after the coastal transition until 75 km offshore, and then continues to increase linearly, but more slowly, without levelling off until the end of the investigated area is reached after a distance of 250 km. For wind directions from S, a similar relationship is observed, but on average the wind speed is 1 m s^{-1} higher than for wind direction from SE. For wind directions from E, the increase of wind speed with distance starts levelling off after around a distance of 200 km offshore.

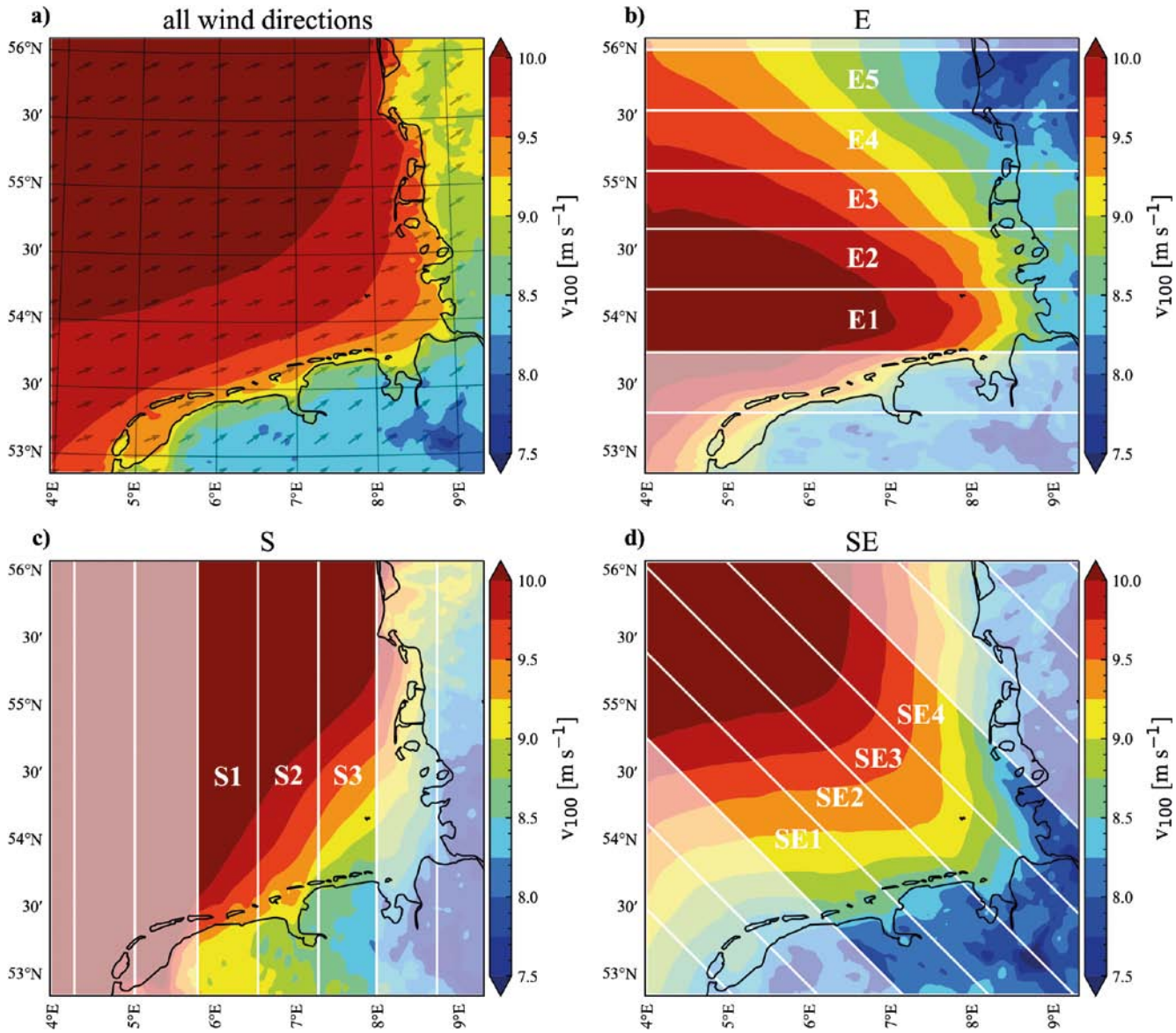

Fig. 1. Average (between 2010 and 2021) wind speed from WRF simulations at a height of 100 m over the German Bight a) averaged over all wind directions, additionally indicating the mean wind direction with arrows, b) averaged over all data with wind direction from E, c) averaged over all data with wind direction from S and, d) averaged over all data with wind direction from SE. The highlighted areas S1, S2, S3, SE1, SE2, SE3, SE4, E1, E2, E3, E4, E5 are selected for the subsequent transect analyses.

3.4 Interannual variability of coastal wind speed

Fig. 4 shows the interannual variability of the wind speed development with distance from the coast at an altitude of 100 m. When all wind directions are taken into account (Fig. 4a), the wind speed above land is between around 8.1 m s^{-1} and 8.9 m s^{-1}, and for the largest distance above water of 250 km considered here, it is between 9.5 m s^{-1} and 10.7 m s^{-1} for individual years. For only offshore wind directions (Fig. 4b), the wind speed above land is in the range of around 7.7 m s^{-1} and 9.0 m s^{-1}, and for distances of 250 km, the wind speed is between 9.3 m s^{-1} and 11.0 m s^{-1} for individual years.

In summary, the wind speed at a distance of 250 km for only offshore wind directions shows a slightly larger interannual variability of up to 1.5 m s^{-1}, compared to the wind speed at a distance of 250 km for all wind directions with an interannual variability of up to 1 m s^{-1}.

3.5 Seasonal and diurnal variability of the coastal transition

The seasonal and diurnal variations of the extent of the coastal transition and the wind speed increase along the transects of directions E, S, and SE are shown for all wind directions in Fig. 5, and for only offshore wind directions in Fig. 6.

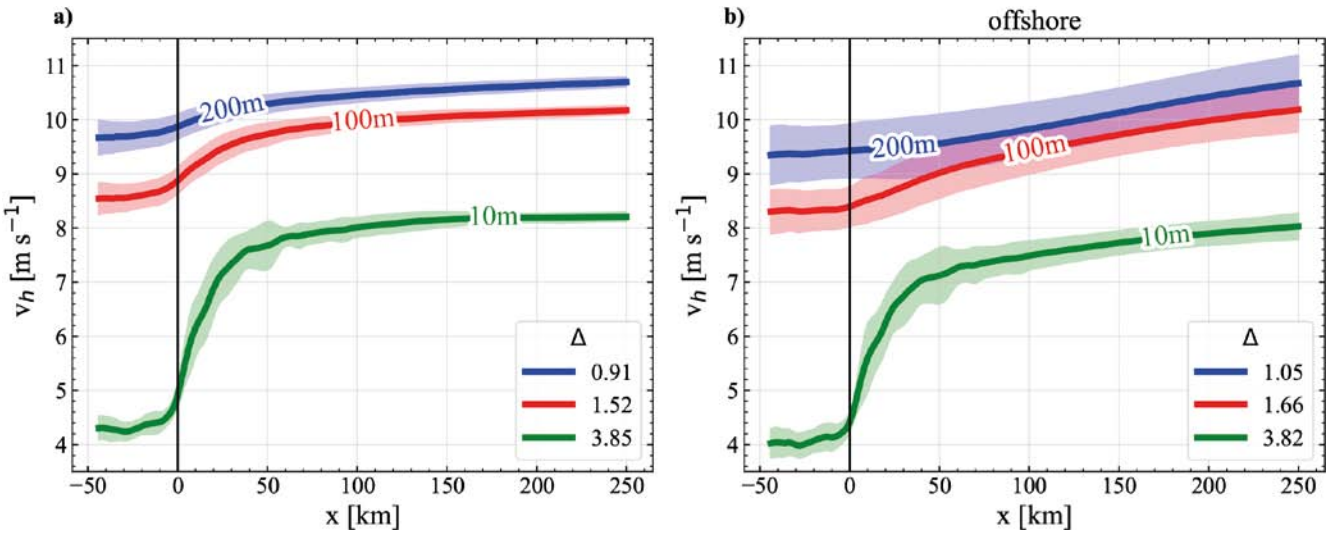

Fig. 2. Average wind speed development across the coast at the height of 10 m (green), 100 m (red) and 200 m (blue). The lines are temporally averaged between 2010 and 2021 and spatially averaged over the transects S1, S2, S3, SE1, SE2, SE3, SE4, E1, E2, E3, E4, E5 shown in Fig. 1. Each transect is averaged orthogonal to its orientation. The unified transect distance dimension x represents land or water for $x < 0$ and $x > 0$. The left panel is averaged over all wind directions (a). The right panel is averaged only over offshore wind directions (b). Δ indicates the difference between the wind speed at 200 km distance and the coastal region at a distance of x = 0 km in m s^{-1}.

Table 2. Development of the wind speed with distance from the coast for the different altitudes 10 m, 100 m and 200 m for all wind directions. The symbol v_{200} indicates the reference wind speed at a distance of 200 km from the coast. The third column calculates 95% of the reference wind speed. The last column shows after which distance 95% of the reference wind speed is reached.

Altitude	v_{200}	95%	distance
10 m	8.2 m s^{-1}	7.8 m s^{-1}	60 km
100 m	10.1 m s^{-1}	9.6 m s^{-1}	35 km
200 m	10.6 m s^{-1}	10.1 m s^{-1}	20 km

Table 3. Development of the wind speed with distance from the coast as in Table 2, but only for offshore wind directions from E, SE, and E.

Altitude	v_{200}	95%	distance
10 m	7.9 m s^{-1}	7.5 m s^{-1}	100 km
100 m	10.0 m s^{-1}	9.5 m s^{-1}	110 km
200 m	10.4 m s^{-1}	9.9 m s^{-1}	115 km

For all wind directions, the increase of the wind speed Δv_h between the coast and a distance of 200 km is highest for the lowest altitude of 10 m, and lowest for the altitude of 200 m (Fig. 5a). Further, the dataset is analyzed separately for the different seasons and day/night time. There is a strong similarity of the wind speed increase for spring, summer and daytime, compared to autumn, winter and nighttime conditions (Fig. 5a). The wind speed reaches 95% of the final value at a distance of 200 km offshore after different distances between 25 and 40 km offshore for all altitudes in spring and summer, while it takes up to 60–80 km for the wind speed at 10 m altitude to reach 95% of the final wind speed. Day and night time do not show large differences at the altitude of 10 m, but the final wind speed at 100 m altitude is reached significantly faster during night, and immediately at 200 m altitude.

For taking into account only offshore wind directions (Fig. 6), the wind speed increase between the coast and a distance of 200 km is generally slightly higher on average, with an increase of 1.1, 1.5, 1.7 m s^{-1} at the heights of 10, 100, 200 m for Δv_h compared to all wind directions. However, the distances Δx_h for reaching 95% of the final wind speed above water is significantly higher than for all wind directions, with

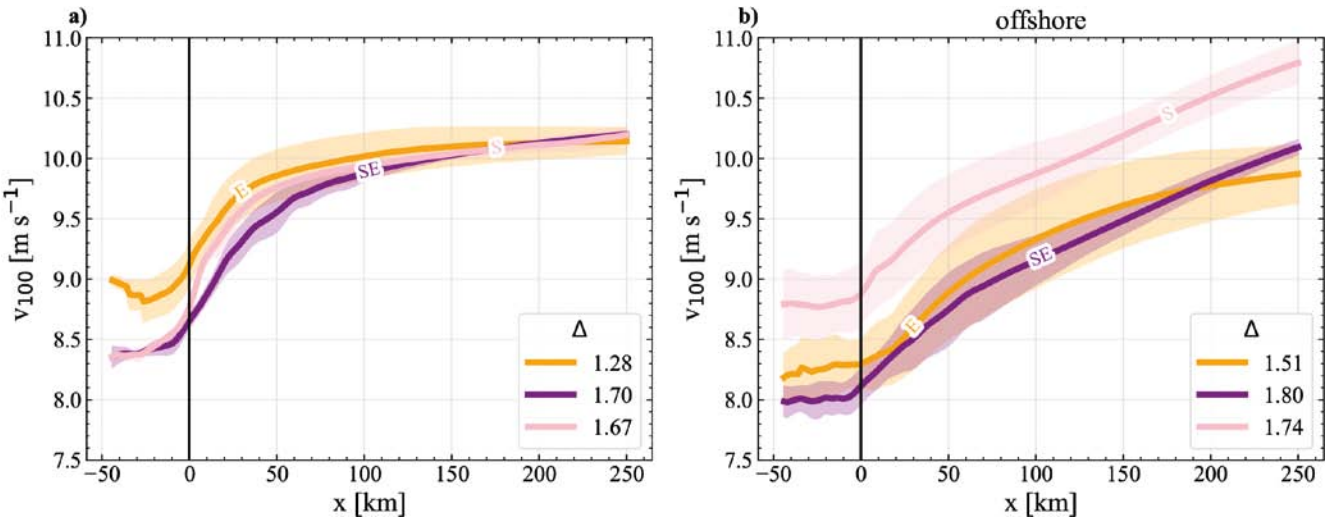

Fig. 3. The coastal wind speed gradient at a height of 100 m for the transect orientations: E (yellow), SE (purple), and S (pink). The transects are shown in Fig. 1. The left panel is averaged over all wind directions (a). The right panel is averaged only over offshore conditions (b). The wind speed at a height of 100 m is plotted against the unified transect distance dimension x, which represents land or water for $x < 0$ and $x > 0$. The coastal transition is at $x = 0$. Δ indicates the difference between the wind speed at 200 km distance and the coastline at x = 0 km in m s^{-1}.

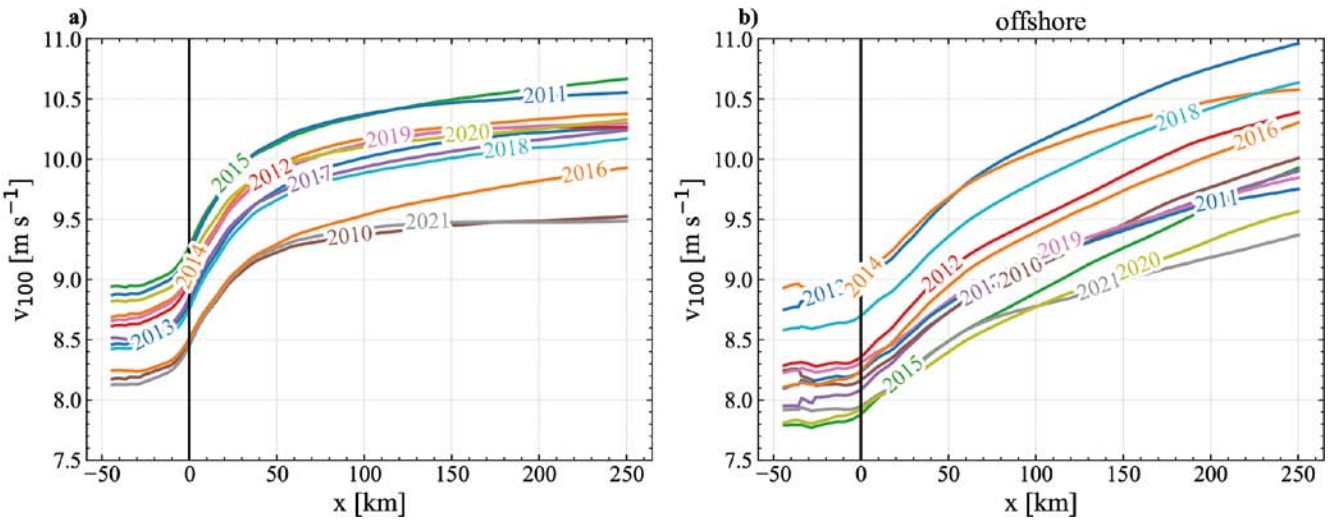

Fig. 4. Interannual variability of the coastal wind speed gradient at a height of 100 m. The left panel is averaged over all wind directions for the years between 2010 and 2021 (a). The right panel is averaged only over offshore wind directions (b).

a wind speed increase of 2.3, 3, 2.5 m s^{-1} at the heights of 10, 100, 200 m for Δx_h. Furthermore, Δx_h decreases with height for the results with all wind directions (Fig. 5b), but increases for offshore wind directions only (Fig. 6b). There are large differences for the seasons and time of day, with generally larger distances to reach the final wind speed for spring, summer and day time, which corresponds to presumably stable atmospheric conditions, as the sea surface temperature is normally lower than the air temperature originating from warmer land masses.

An overview of all numerical experiments, separating between day and night, as well as the four seasons, each case for all wind directions and for only offshore wind directions, is provided in the appendix (Fig. A.1).

3.6 Normalization of the wind speed

An approach to take into account the variability of the wind speed caused by large scale phenomena, such as synoptic scale differences, is to normalize with respect to the wind speed at the height of 1 km, which is the top of the WRF

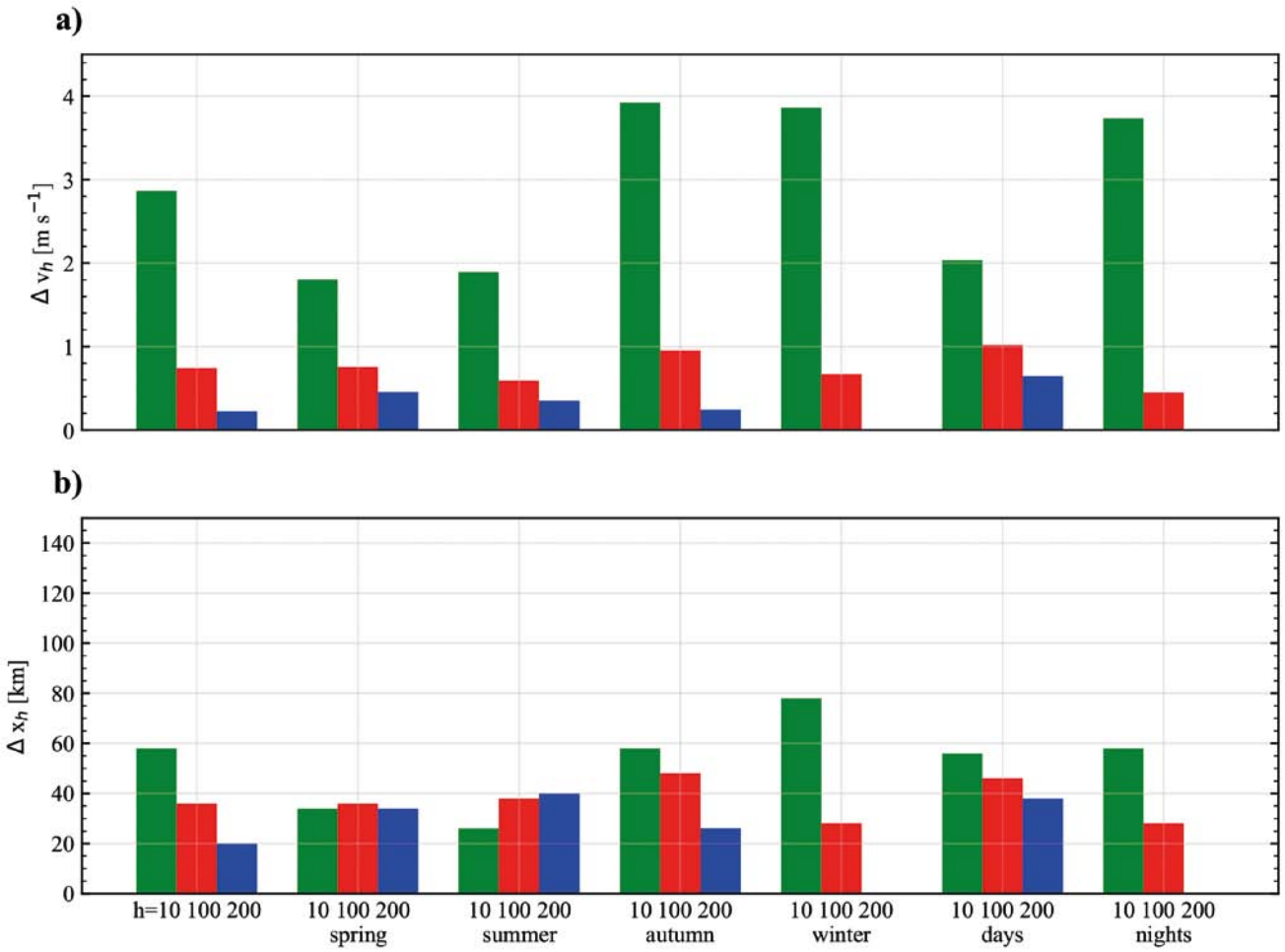

Fig. 5. Difference of the wind speed from the coast to a distance of 200 km (a) and distance to reach 95% of the wind speed at a distance of 200 km (b) averaged over **all wind directions**. The data are additionally divided into season and day/night time. Further, each data set is divided into the three heights 10 m (green), 100 m (red) and 200 m (blue).

domain and can be considered as part of the free atmosphere. The free atmosphere is not influenced by the surface and boundary layer effects, but by the large scale synoptic pressure distributions. Therefore, the normalization to the wind speed at 1 km altitude was used to remove the dependence on the synoptic wind speed. Similar to the absolute wind speed shown in Fig. 2, the wind speed normalized to 1 km height also indicates that the wind speed near the coast is generally lower than over open sea (see appendix, Fig. A.2). The wind speed gradient follows the shape of the coastline, but is more pronounced on the southern coast towards the prevailing wind direction. For easterly wind directions (E), the wind field shows a faster increase in wind speed with higher values at 54 °N, where the landmass is thinnest to the east. Here, higher wind speed is observed near the coast. For southerly wind directions (S), the new equilibrium wind speed is reached over shorter distances towards the west. For southeast wind directions (SE), the lines of equal wind speed trace the shape of the coastline, and the influence of the coastal transition on the wind field can be estimated to extend up to 200 km offshore. The results for wind speed from easterly and southerly directions show very site-specific features, while the results for southeast wind direction show a continuous increase in wind speed along both coastlines.

Compared to the absolute values of wind speed, the final relative wind speed (defined at a distance of 200 km) is reached earlier, both for all wind directions and for only offshore wind directions. The average increase in wind speed from the coast to a distance of 200 km is slightly higher for only offshore wind directions than for all wind directions.

Furthermore, the wind speed ratio for the altitudes of 100 m and 200 m becomes greater than 1, implying on average higher wind speed at 100 m and at 200 m than at 1000 m, which is more pronounced for only offshore wind directions. Such flow conditions indicate the existence of a low-level jet, which is particularly frequent for offshore wind direc-

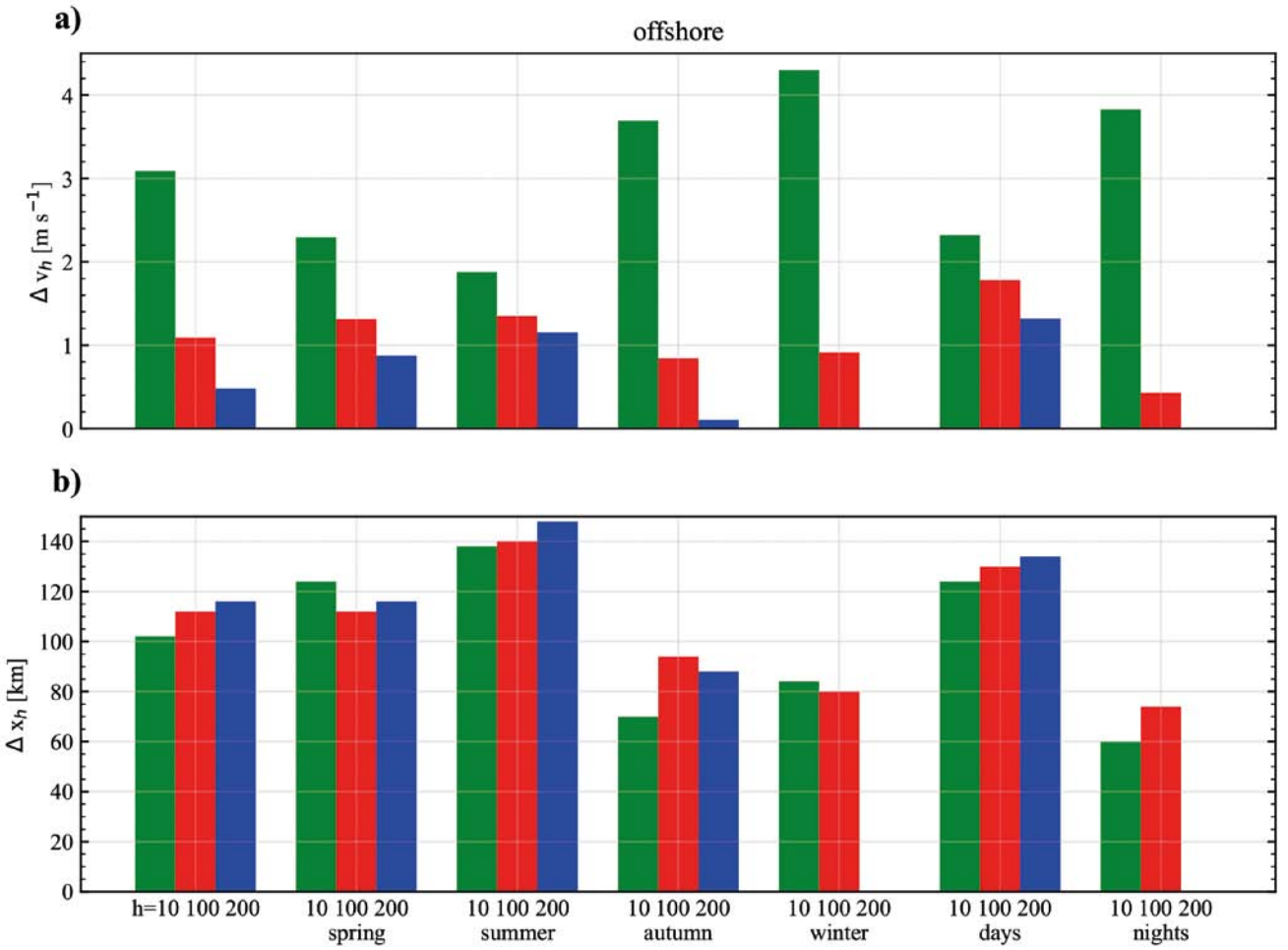

Fig. 6. Difference of the wind speed from the coast to a distance of 200 km (a) and distance to reach 95% of the wind speed at a distance of 200 km (b) averaged over **only offshore wind directions** from S, SE, E. The data are additionally divided into season and day/night time. Further, each data set is divided into the three heights 10 m (green), 100 m (red) and 200 m (blue).

tions and stable conditions. Fig. 7 gives an estimate of the areas with ratios greater than 1. This is further investigated in the partner paper Barekzai et al. (2024).

3.7 Summary of results

In summary, the analyses provide insight on the influence of various parameters on the wind speed across the coastal transition:

- Distance from the coast: Generally, wind speed increases with distance from the coast. This is due to the coastal effect, which arises from the transition from the rough land surface to the smoother water surface.
- Wind direction: Wind speed development varies with wind direction. For offshore wind directions, the increase in wind speed with distance from the coast is more pronounced compared to the average over all wind directions. This is because offshore winds flow directly from the land surface to the water surface, experiencing the coastal effect more strongly.
- Height: Wind speed increases with height. This effect is more pronounced near the coast than over open water.
- Season: The coastal effect is stronger during spring and summer than in autumn and winter. This could be due to the different temperature differences between land and water during the various seasons.
- Time of day: Wind speed development also shows differences between day and night, although these differences are less pronounced than seasonal variations.

4 Discussion

The analyses show that for offshore wind directions, it takes a much longer distance for the wind speed to reach a new equilibrium above the open water than for taking into account all wind directions. For all three altitudes investigated here, a linear increase of the wind speed from near the coast to beyond 200 km was still observed. For offshore wind

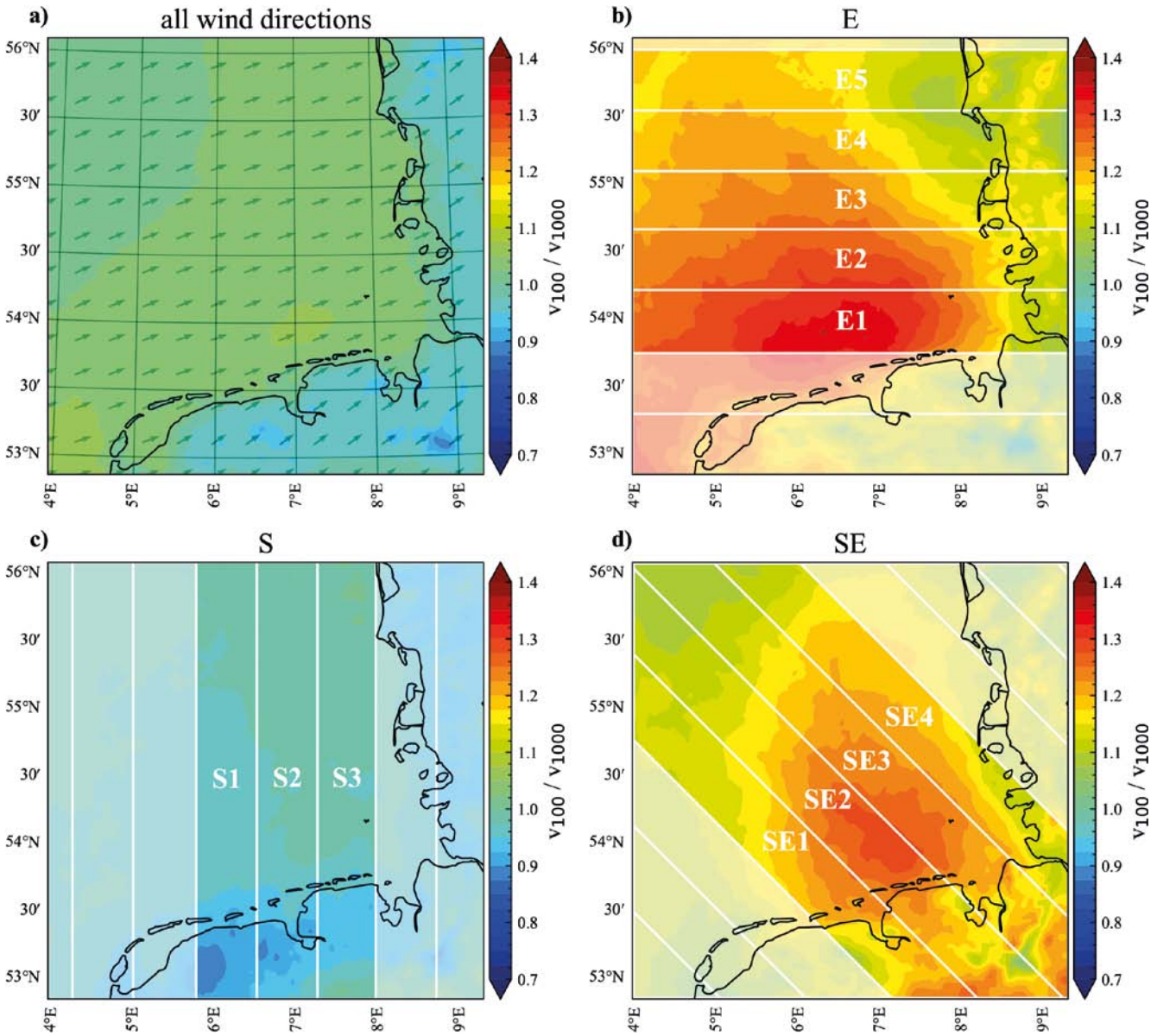

Fig. 7. Average wind speed from WRF simulations normalized to the wind speed at a height of 1 km, represented at a height of 100 m. For further information, see Fig. 1.

directions, the increase of the wind speed was particularly pronounced during spring and summer, and during daytime, compared to all wind directions. This indicates that stable atmospheric conditions play an important role for the coastal effect: in spring and summer, the sea surface temperature is relatively cold compared to air masses warmed up above land, which are then advected over the colder surface for offshore wind directions, creating a temperature inversion of warmer air masses above colder near-surface air masses. This is most pronounced during day time. This phenomenon of stable stratification has been investigated in depth for the German Bight, as stable conditions are associated with long-reaching wind park wakes as well (Cañadillas et al. 2020). Stable atmospheric conditions have been estimated to occur in total a time of around 37% of the year in the German Bight (Emeis et al. 2016). The development of an internal boundary layer for stable conditions results in longer distances until the new equilibrium wind speed above the open sea is reached, which has been shown by different methods, e.g. the analysis of satellite-derived wind speed (Djath et al. 2022), experimental studies (Smedman et al. 1997) and numerical simulations (Dörenkämper et al. 2015). The importance of stable atmospheric conditions requires particular attention on the correct representation in numerical simulations. It is well-known that the WRF model tends to forecast more moderately stable stratifications compared to

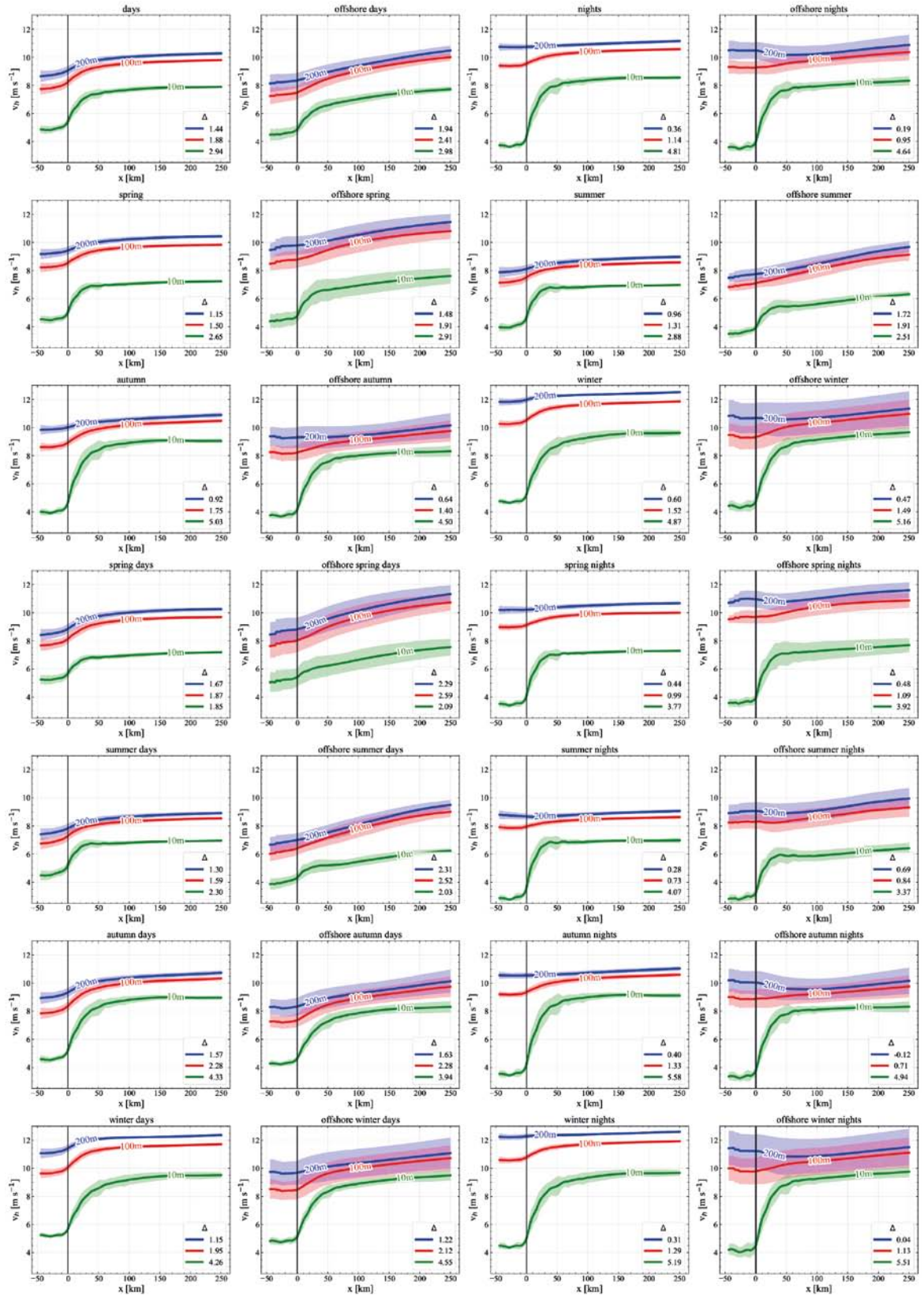

Fig. A.1. Summary of the experiments, showing the wind speed development from the coast to the open sea at several heights (10 m in green, 100 m in red, 200 m in blue) and divided by different conditions, all wind directions, only offshore wind directions, seasons, day and nighttime. The difference Δ in m s^{-1} between the wind speed at the coast and at a distance of 200 km is provided.

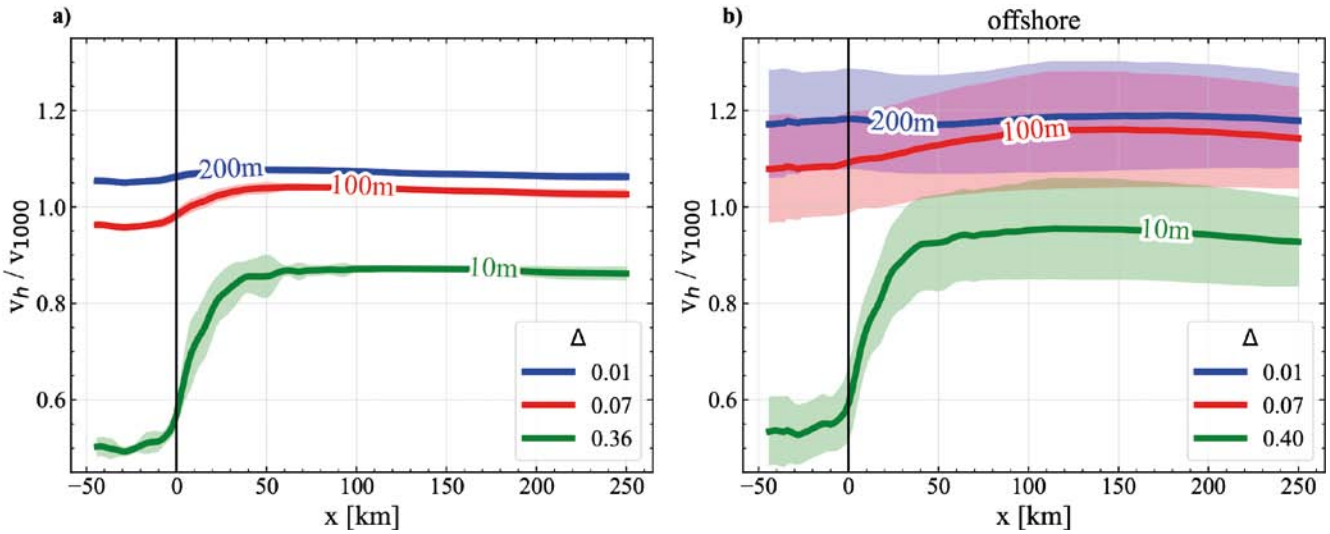

Fig. A.2. Average wind speed from WRF simulations, normalized to the wind speed at a height of 1 km. Δ indicates the difference between the normalized wind speed at 200 km distance and the coastline at x = 0 km. For further information, see Fig. 2.

measurements and a reinforcement of the instability under neutral and convective regimes. Stable conditions are the most complicated scenario for the atmospheric boundary layer schemes implemented in the model to reproduce due to their overdiffusive formulations (Muñoz-Esparza et al. 2012b).

5 Conclusion

In summary, the dependence of the wind speed gradient from the coast to the open sea on wind direction was investigated based on a 12-year WRF reanalysis data set of the German Bight area. The wind speed development from the coast to the open sea was analyzed for the average over all wind directions, and for only offshore wind directions, for the altitudes of 10 m, 100 m and 200 m. The key findings are as follows:

- The coastal transition has effects on scales ranging from several tens of kilometers to over 200 kilometers.
- For offshore wind directions, the wind speed requires a much larger distance to reach a new equilibrium over open water.
- A linear increase in wind speed from the coast to over 200 kilometers was still observed for all three examined altitudes (10 m, 100 m, and 200 m).
- For offshore wind directions, the increase in wind speed was particularly pronounced in spring and summer, as well as during the day, compared to all wind directions.
- This suggests that stable atmospheric conditions play an important role in the coastal effect.
- The development of an internal boundary layer under stable conditions leads to larger distances before the new equilibrium wind speed is reached over open water.

The study quantifies the wind speed gradient for different altitudes and wind directions for a large data set. Understanding this phenomenon is highly relevant for wind energy. Current wind turbines in the German Bight have a hub height of around 100 m. Therefore, they are influenced by the flow between the surface and an altitude of around 200 m. Since most of the wind turbines currently installed in the German Bight are less than 200 km from the nearest coastline (Schulz-Stellenfleth et al. 2022b), they are significantly affected by the coastal effect for certain wind directions.

The wind speed gradient influenced by the internal boundary layer has a direct influence on the available wind resource and therefore the power production of offshore wind turbines (Barthelmie et al. 2007).

Acknowledgments: The project X-Wakes was funded by the German Federal Ministry of Economic Affairs and Energy (BMWi), now Federal Ministry for Economic Affairs and Climate Action (BMWK) under grant number FKZ 03EE3008B on the basis of a decision by the German Bundestag.

A Appendix

An additional figure with a comprehensive overview of all experiments is shown (Fig. A.1), and an illustration of the development of the normalized wind speed (Fig. A.2).

References

Akhtar, N., Geyer, B., Rockel, B., Sommer, P. S., & Schrum, C. (2021). Accelerating deployment of offshore wind energy alter wind climate and reduce future power generation potentials. *Scientific Reports, 11*(1), 11826. https://doi.org/10.1038/s41598-021-91283-3

Atkinson, B. W. (1981). *Meso-scale Atmospheric Circulations*. London: Academic Press.

Barekzai, M., Cañadillas, B., Emeis, S., Dörenkämper, M., & Lampert, A. (2024). Mesoscale simulations of coastal boundary-layer transitions. Part 1: Low-level jets. *Meteorologische Zeitschrift*. https://doi.org/10.1127/metz/2024/1195

Barthelmie, R., Badger, J., Pryor, S., Hasager, C., Christiansen, M., & Jørgensen, B. (2007). Offshore coastal wind speed gradients: Issues for the design and development of large offshore windfarms. *Wind Engineering, 31*(6), 369–382. https://doi.org/10.1260/030952407784079762

Cañadillas, B., Foreman, R., Barth, V., Siedersleben, S., Lampert, A., Platis, A., … Neumann, T. (2020). Offshore wind farm wake recovery: Airborne measurements and its representation in engineering models. *Wind Energy, 23*(5), 1249–1265. https://doi.org/10.1002/we.2484

Cañadillas, B., Wang, S., Ahlert, Y., Djath, B., Barekzai, M., Foreman, R., & Lampert, A. (2023). Coastal horizontal wind speed gradients in the North Sea based on observations and ERA5 reanalysis data. *Meteorologische Zeitschrift, 32*(3), 207–228. https://doi.org/10.1127/metz/2022/1166

Cheynet, E., Solbrekke, I. M., Diezel, J. M., & Reuder, J. (2022). A one-year comparison of new wind atlases over the North Sea. *Journal of Physics: Conference Series, 2362*(1), 012009. https://doi.org/10.1088/1742-6596/2362/1/012009

Djath, B., Schulz-Stellenfleth, J., & Cañadillas, B. (2022). Study of coastal effects relevant for offshore wind energy using spaceborne synthetic aperture radar (SAR). *Remote Sensing, 14*(7), 1688. https://doi.org/10.3390/rs14071688

Dörenkämper, M., Witha, B., Steinfeld, G., Heinemann, D., & Kühn, M. (2015). The impact of stable atmospheric boundary layers on wind-turbine wakes within offshore wind farms. *Journal of Wind Engineering and Industrial Aerodynamics, 144*, 146–153. https://doi.org/10.1016/j.jweia.2014.12.011

Dörenkämper, M., Olsen, B. T., Witha, B., Hahmann, A. N., Davis, N. N., Barcons, J., … Mann, J. (2020). The making of the New European Wind Atlas – part 2: Production and evaluation. *Geoscientific Model Development, 13*(10), 5079–5102. https://doi.org/10.5194/gmd-13-5079-2020

Emeis, S., Siedersleben, S., Lampert, A., Platis, A., Bange, J., Djath, B., … Neumann, T. (2016). Exploring the wakes of large offshore wind farms. *Journal of Physics: Conference Series, 753*, 092014. https://doi.org/10.1088/1742-6596/753/9/092014

European Wind Energy Association (2013). Wind in power, 2012 European Statistic. *Technical report*.

Gottschall, J., & Dörenkämper, M. (2021). Understanding and mitigating the impact of data gaps on offshore wind resource estimates. *Wind Energy Science, 6*(2), 505–520. https://doi.org/10.5194/wes-6-505-2021

Gualtieri, G. (2021). Reliability of ERA5 reanalysis data for wind resource assessment: A comparison against tall towers. *Energies, 14*(14), 4169. https://doi.org/10.3390/en14144169

Hasager, C. B., Hahmann, A. N., Ahsbahs, T., Karagali, I., Sile, T., Badger, M., & Mann, J. (2020). Europe's offshore winds assessed with synthetic aperture radar, ASCAT and WRF. *Wind Energy Science, 5*(1), 375–390. https://doi.org/10.5194/wes-5-375-2020

International Energy Agency (2022). World energy outlook 2022. *Technical report*.

Kumar, R., Stallard, T., & Stansby, P. K. (2021). Large-scale offshore wind energy installation in northwest india: Assessment of wind resource using weather research and forecasting and levelized cost of energy. *Wind Energy, 24*(2), 174–192. https://doi.org/10.1002/we.2566

Lampert, A., Bärfuss, K., Platis, A., Siedersleben, S., Djath, B., Cañadillas, B., … Emeis, S. (2020). In situ airborne measurements of atmospheric and sea surface parameters related to offshore wind parks in the German Bight. *Earth System Science Data, 12*(2), 935–946. https://doi.org/10.5194/essd-12-935-2020

Lampert, A., Hankers, R., Feuerle, T., Rausch, T., Cremer, M., Angermann, M., … Bärfuss, K. B. (2024). In situ airborne measurements of atmospheric parameters and airborne sea surface properties related to offshore wind parks in the German Bight during the project X-Wakes. *Earth System Science Data, 16*(10), 4777–4792. https://doi.org/10.5194/essd-16-4777-2024

Larsén, X. G., & Fischereit, J. (2021). A case study of wind farm effects using two wake parameterizations in the weather research and forecasting (WRF) model (v3.7.1) in the presence of low-level jets. *Geoscientific Model Development, 14*(6), 3141–3158. https://doi.org/10.5194/gmd-14-3141-2021

Larsén, X. G., Fischereit, J., Hamzeloo, S., Bärfuss, K., & Lampert, A. (2024). Investigation of wind farm impacts on surface waves using coupled numerical simulations. *Renewable Energy, 237*, 121671. https://doi.org/10.1016/j.renene.2024.121671

Lee, J. C. Y., & Lundquist, J. K. (2017). Evaluation of the wind farm parameterization in the weather research and forecasting model (version 3.8.1) with meteorological and turbine power data. *Geoscientific Model Development, 10*(11), 4229–4244. https://doi.org/10.5194/gmd-10-4229-2017

Li, H., Claremar, B., Wu, L., Hallgren, C., Körnich, H., Ivanell, S., & Sahlée, E. (2021). A sensitivity study of the WRF model in offshore wind modeling over the Baltic Sea. *Geoscience Frontiers, 12*(6), 101229. https://doi.org/10.1016/j.gsf.2021.101229

Lundquist, J., Duvivier, K. K., Kaffine, D., & Tomaszewski, J. M. (2018). Costs and consequences of wind turbine wake effects arising from uncoordinated wind energy development. *Nature Energy, 4*(1), 26–34. https://doi.org/10.1038/s41560-018-0281-2

Manzano-Agugliaro, F., Sanchez-Calero, M., Alcayde, A., San-Antonio-Gomez, C., Perea-Moreno, A. J., & Salmeron-Manzano, E. (2020). 2020: Wind turbine offshore foundations and connections to grid. *Inventions, 5*(1), 8. https://doi.org/10.3390/inventions5010008

Muñoz-Esparza, D., Cañadillas, B., Neumann, T., & van Beeck, J. (2012a). Turbulent fluxes, stability and shear in the offshore environment: Mesoscale modelling and field observations at FINO1. *Journal of Renewable and Sustainable Energy, 4*(6), 063136. https://doi.org/10.1063/1.4769201

Muñoz-Esparza, D., Cañadillas, B., Neumann, T., & Beeck, J. (2012b). Turbulent fluxes, stability and shear in the offshore environment: Mesoscale modelling and field observations at FINO1. *Journal of Renewable and Sustainable Energy, 4*(6), 063136. https://doi.org/10.1063/1.4769201

Platis, A., Hundhausen, M., Mauz, M., Siedersleben, S., Lampert, A., Bärfuss, K., … Bange, J. (2021). Evaluation of a simple analytical model for offshore wind farm wake recovery by in situ data and weather research and forecasting simulations. *Wind Energy, 24*(3), 212–228. https://doi.org/10.1002/we.2568

Rausch, T., Cañadillas, B., Hampel, O., Simsek, T., Tayfun, Y. B., Neumann, T., … Lampert, A. (2022). Wind lidar and radiosonde measurements of low-level jets in coastal areas of the German Bight. *Atmosphere, 13*(5), 839. https://doi.org/10.3390/atmos13050839

Sandu, I., Beljaars, A., Bechtold, P., Mauritsen, T., & Balsamo, G. (2013). Why is it so difficult to represent stably stratified conditions in numerical weather prediction (NWP) models? *Journal of Advances in Modeling Earth Systems, 5*(2), 117–133. https://doi.org/10.1002/jame.20013

Schulz-Stellenfleth, J., Emeis, S., Dörenkämper, M., Bange, J., Cañadillas, B., Neumann, T., … Lampert, A. (2022a). Coastal impact on offshore wind farms – a review focusing on the German Bight area. *Meteorologische Zeitschrift, 31*(4), 289–315. https://doi.org/10.1127/metz/2022/1109

Schulz-Stellenfleth, J., Emeis, S., Dörenkämper, M., Bange, J., Cañadillas, B., Neumann, T., … Lampert, A. (2022b). Coastal impacts on offshore wind farms – a review focussing on the German Bight area. *Meteorologische Zeitschrift, 31*(4), 289–315. https://doi.org/10.1127/metz/2022/1109

Siedersleben, S. K., Platis, A., Lundquist, J. K., Lampert, A., Bärfuss, K., Cañadillas, B., … Emeis, S. (2018). Evaluation of a wind farm parametrization for mesoscale atmospheric flow models with aircraft measurements. *Meteorologische Zeitschrift, 27*(5), 401–415. https://doi.org/10.1127/metz/2018/0900

Skamarock, C., Klemp, B., Dudhia, J., Gill, O., Liu, Z., Berner, J., Wang, W., Powers, G., Duda, G., Barker, D.M., & Huang, X. (2019). A Description of the Advanced Research WRF Model Version 4. https://doi.org/10.5065/1dfh-6p97

Smedman, A. S., Tjernström, M., & Högström, U. (1993). Analysis of the turbulent structure of a marine low-level jet. *Boundary-Layer Meteorology, 66*, 105–126. https://doi.org/10.1007/BF00705462

Smedman, A. S., Bergström, H., & Grisogono, B. (1997). Evolution of stable internal boundary layers over a cold sea. *Journal of Geophysical Research, 102*(C1), 1091–1099. https://doi.org/10.1029/96JC02782

Steele, C. J., Dorling, S. R., Von Glasow, R., & Bacon, J. (2015). Modelling sea-breeze climatologies and interactions on coasts in the southern North Sea: Implications for offshore wind energy. *Quarterly Journal of the Royal Meteorological Society, 141*(690), 1821–1835. https://doi.org/10.1002/qj.2484

van der Laan, M., Peña, A., Volker, P., Hansen, K. S., Sørensen, N. N., Ott, S., & Hasager, C. B. (2017). Challenges in simulating coastal effects on an offshore wind farm. *Journal of Physics: Conference Series, 854*, 012046. https://doi.org/10.1088/1742-6596/854/1/012046

Wiser, R., Rand, J., Seel, J., Beiter, P., Baker, E., Lantz, E., & Gilman, P. (2021). Expert elicitation survey predicts 37% to 49% declines in wind energy costs by 2050. *Nature Energy, 6*(5), 555–565. https://doi.org/10.1038/s41560-021-00810-z

WRF Users Page (2020). WRF model physics options and references. last accessed: 13.07.2020.

Manuscript received: March 21, 2023
Revisions requested: September 10, 2024
Revised version received: December 6, 2024
Manuscript accepted: December 12, 2024